Appendix A: Flatfile Documentation

1 Introduction

The FDHI Database contains data and metadata on earthquake characteristics, fault displacement observations, and surface rupture mapping are stored in a relational database across 37 tables and 365 columns. A relational database is ideal for organizing large amounts of interrelated data, but it requires knowledge of the database schema to extract information. To better support end-users of the FDHI Database, including model developers and the wider geoscience community, the database contents have been aggregated into flatfiles. The flatfiles are considered the formal documentation of the database contents.

The FDHI Database flatfiles and related digital products are publicly available at https://doi.org/10.25346/S6/Y4F9LJ. The flatfiles are provided in comma-separated (CSV) file format, and the related digital products provide the flatfiles in map-based formats (i.e., Esri shapefiles, and Google Earth KMZ files.)

Separate are provided for different data geometries when necessary. For example, mapped surface ruptures are lines whereas fault displacement measurement sites are points, so these are contained in separate CSV and SHP files. The KMZ format allows multiple geometries, so the lines and points do not need to be in separate files. The reference line (ECS) axes that serve as the basis for the event-specific coordinates are provided separate from the rupture and measurement data. A file containing column definitions and necessary metadata is also provided as an Excel spreadsheet. Accordingly, eight files are included when the *FDHI Database flatfiles and related digital products* is downloaded:

1. **01_FDHI_FLATFILE_DEFINITIONS.xlsx** – This file defines the columns in the measurements, ruptures, and ECS files.
2. **02_FDHI_FLATFILE_MEASUREMENTS.csv** – Fault displacement measurement data and metadata in CSV format.
3. **03_FDHI_FLATFILE_RUPTURES.csv** – Mapped surface rupture data and metadata in CSV format.
4. **04_FDHI_FLATFILE_ECS.csv** – Event coordinate system reference lines and metadata in CSV format.
5. **05_FDHI_FLATFILE_MEASUREMENTS.shp.zip** – Fault displacement measurement data and metadata in Esri shapefile format.

6. **06_FDHI_FLATFILE_RUPTURES.shp.zip** – Mapped surface rupture data and metadata in Esri shapefile format.
7. **07_FDHI_FLATFILE_ECS.shp.zip** – Event coordinate system data and metadata in Esri shapefile format.
8. **08_FDHI_Event_KMZ.zip** – Data and metadata for fault displacement measurements, mapped surface ruptures, and event coordinate systems in one KMZ file.

The Chapters in this Appendix provide information on the database flatfiles, related digital products, and the citations for the data sources used in the database. Chapter 2 summarizes the definitions file and flatfile contents. Chapter 3 describes the related products, which are map-based formats of the flatfiles. Data plots are available as an electronic supplement to this Appendix, as described in Chapter 4. The software used to generate database flatfiles, related digital products, and data plots is documented in Chapter 5. Finally, full citations for all data sources in the database are listed in Chapter 6.

2 Flatfile Descriptions

The FDHI Database contains three flatfiles because there are three distinct data collections or categories. The distinction is based on the spatial dimensionality of the data and the data contents. The Measurements Flatfile contains data and metadata associated with "a point in space," where the points are a measurement location. The Ruptures Flatfile contains data and metadata associated with "a line in space," where the lines are mapped surface ruptures. The ECS Flatfile contains data and metadata associated with "a line in space," where the lines are the reference linepath of the ECS coordinate systems. The ECS is a two-dimensional reference line that accounts for curvature and discontinuities in the full surface rupture expression, including rupture traces and measurement locations. Chapter 4.5 of the main report described the development of the ECS.

The flatfiles are provided in CSV format at https://doi.org/10.25346/S6/Y4F9LJ. We also include a Definitions file in electronic format that contains the definitions of each column in each flatfile and the dataset citations with flatfiles.

2.1 DEFINITIONS FILE

The Definitions file (*.xlsx format; File #01 in *FDHI Database flatfiles and related digital products*) contains the column definitions for all three flatfiles and the database citations. The information is split across six tabs in the Excel sheet:

1. MEASUREMENTS_FLATFILE
2. quality_code_explanation
3. group_id_explanation
4. RUPTURES_FLATFILE
5. ECS_FLATFILE
6. CITATIONS

The contents of the first three tabs are repeated in Tables A.1, A.2, and A.3 in Chapter 2.2 of this Appendix. The fourth and fifth tabs are also in Tables A.4 and A.5 (Appendix Chapters 2.3 and 2.4, respectively). The citations are also repeated in Chapter 6 of this Appendix.

2.2 MEASUREMENTS FLATFILE

The Measurements Flatfile (*.csv format; File #02 in *FDHI Database flatfiles and related digital products*) contains 136 columns to capture the metadata, raw data, and interpreted data. The main report describes the data collection and data analysis/interpretation procedures. Table A.1 shows the column names in the *.csv flatfile with the column definitions. The equivalent column names in the ESRI shapefile (discussed more in Chapter 3 of this Appendix) are also listed in Table A.1. The information in Table A.1 also contained in the Definitions file (File #01; see Chapter 2.1 of this Appendix).

For convenience, a unique row index was added to the flatfile. If the index is disregarded, then unique entries in the Measurements Flatfile are determined by five columns (i.e., a composite primary key): EQ_ID, PT_DS_ID, PT_ID, MEAS_ID, and RUP_DS_ID.

It is noted that some events have multiple (alternative) rupture datasets; therefore, the RUP_DS_ID column is part of the composite primary key. This also means that measurement entries are repeated when there are multiple rupture datasets.

As part of our quality review program, we evaluated each measurement for accuracy and consistency to develop a recommended net slip value for use in model development. More information on the development of these recommendations is in Chapter 4.6.2 of the main report. The results of this evaluation are reflected in the Measurements Flatfile in four columns:

1. recommended_net_preferred_for_analysis_meters
2. recommended_net_vector_basis
3. recommended_net_usage_flag
4. quality_code

The first column is the best-estimate net displacement (in meters) based on the reported slip components, and the second column lists the slip components used in the calculation. The third column provides guidance on the usage of the recommended net displacement (Keep, Check, or Toss) to assist the model developers in data screening. The fourth column documents the basis for the Keep/Check/Toss recommendation through our custom quality codes (Table A.2). If a data point is labeled "Check" with a quality code of 2000 or 2001, that indicates there is a technically defensible alternative measurement available at approximately the same location. Alternative measurements will have the same "location_id" and "EQ_ID."

Through our quality review program, we also explicitly identified, where applicable, sets of measurements in each earthquake are incompatible due to the measurement techniques or tools used by the dataset originator. We use the "group_id" column to separate the data into recommended sets that are internally compatible. The most common example is differentiating between wide-aperture measurements based on optical image correlation (pixel mapping) and field measurements on a discrete rupture. These measurement techniques are incompatible in model

development because they are measuring different metrics (i.e., wide-aperture versus narrow aperture deformation). Other examples of incompatible measurement metrics include vertical slip versus scarp height, and measurement techniques that might include slip from multiple events. More details on these interpretations are discussed in the main report, and a summary of the "group_id" values is in Table A.3.

Table A.1. Measurements Flatfile column explanation.

Full Name (SQL, Flatfiles)	Short Name (SHP, KMZ)	Datatype	Definition
index	index	integer	Unique row identifier in flatfile for indexing purposes only; not related database primary keys or content
EQ_ID	EQ_ID	integer	Unique identifier for each earthquake
eq_name	EQ_ID2	string	Common name for each earthquake
eq_date	eq_date	string	Earthquake date YYYY-MM-DD
region	region	string	Geographical area of earthquake
magnitude	magnitude	float	Earthquake magnitude
magnitude_type	mag_type	string	Earthquake magnitude type: Mw = moment magnitude; Mwc = moment magnitude derived from centroid moment tensor inversion of long-period surface waves; Mww = moment magnitude derived from centroid moment tensor inversion of W-phase; mB = body-wave magnitude; ML = local magnitude; Ms = surface-wave magnitude; U = unspecified
style	style	string	Dominant earthquake style
multi_event_flag	multievent	integer	Indicates if dataset-event pair captures one or more earthquakes for which data cannot be attributed to individual events (0 = no; 1 = yes, multi-event)
aftershock_flag	aftershock	integer	Indicates if measurement is known to have ruptured in an aftershock (0 = no; 1 = yes, aftershock)
hypocenter_longitude_degrees	hypo_long	float	Earthquake hypocenter longitude [decimal degrees]
hypocenter_latitude_degrees	hypo_lat	float	Earthquake hypocenter latitude [decimal degrees]
hypocenter_depth_km	hypo_depth	float	Earthquake hypocenter depth [km]
epsg_for_analysis	epsg	integer	Datum and projection identification number per European Petroleum Search Group (EPSG) standard; recommended projection for analysis in meters
PT_DS_ID	PT_DS_ID	integer	Dataset unique identifier for measurement data
dataset_completion	completion	string	Description of dataset-event pair completion
mapping_scale	map_scale	string	Description of dataset mapping scale
PT_ID	PT_ID	integer	Semi-unique identifier for each measurement (for each dataset and each earthquake, values are unique)

Full Name (SQL, Flatfiles)	Short Name (SHP, KMZ)	Datatype	Definition
MEAS_ID	MEAS_ID	integer	Measurement number at each *PT_ID* (i.e., accommodates multiple measurements at same site); for each measurement, dataset, and earthquake, values are unique
obs_year	obs_year	integer	Observation (measurement) year
obs_mody	obs_mody	integer	Observation (measurement) month and day
days_elapsed	days_elaps	integer	Number of days elapsed between earthquake and observation (measurement)
obs_date_approx_flag	obs_flag	boolean	Flag = 1 if measurement date is approximate; = 0 if exact
measurement_uncertainty_type	unc_type	string	Description of measurement reported uncertainty (e.g.: 1-sigma, 95% confinence interval, etc.)
location_basis	loc_basis	string	Description of measurement location (latitude/longitude) basis
aperture_max_meters	aper2	float	Measurement aperture width [meters]
latitude_degrees	latitude	float	Measurement latitude (depending on table) [decimal degrees]
longitude_degrees	longitude	float	Measurement longitude (depending on table) [decimal degrees]
originator_id	orig_id	string	Measurement location identifier from original/source dataset
originator_quality_note	orig_qual	string	Measurement quality reported by original/source dataset (e.g.: Low, Medium, High, Medium-High)
measured_feature	feature	string	Measured feature reported by original/source dataset
n_splays	n_splays	string	Number of discrete fault splays captured in measurement (e.g.: Single, Multiple, Unknown)
slip_unknown_lateral_nonzero	NonZeroLat	boolean	Reported tectonic slip, lateral motion, indeterminate amount
slip_unknown_unspecified_nonzero	NonZeroUns	boolean	Reported tectonic slip, unspecified style/motion, indeterminate amount
slip_unknown_vertical_nonzero	NonZeroVrt	boolean	Reported tectonic slip, vertical motion, indeterminate amount
fzw_central_meters	fzw_cen	float	Fault zone width preferred value at measurement site [meters]
fzw_high_meters	fzw_hi	float	Fault zone width high estimate [meters]
fzw_low_meters	fzw_lo	float	Fault zone width low estimate [meters]
fzw_meas_type	fzw_mtype	string	Fault zone width measurement type
fps_central_meters	fps_cen	float	Fault-parallel slip preferred value at measurement site [meters]
fps_high_meters	fps_hi	float	Fault-parallel slip high estimate [meters]
fps_low_meters	fps_lo	float	Fault-parallel slip low estimate [meters]

Full Name (SQL, Flatfiles)	Short Name (SHP, KMZ)	Datatype	Definition
fps_meas_type	fps_mtype	string	Fault-parallel slip measurement type
fps_style	fps_style	string	Fault-parallel slip style: Right-Lateral or Left-Lateral
fns_central_meters	fns_cen	float	Fault-normal slip preferred value at measurement site [meters]
fns_high_meters	fns_hi	float	Fault-normal slip high estimate [meters]
fns_low_meters	fns_lo	float	Fault-normal slip low estimate [meters]
fns_meas_type	fns_mtype	string	Fault-normal slip measurement type
fns_style	fns_style	string	Fault-normal slip style: Extension or Compression
nhs_central_meters	nhs_cen	float	Net horizontal slip preferred value at measurement site [meters]
nhs_high_meters	nhs_hi	float	Net horizontal slip high estimate [meters]
nhs_low_meters	nhs_lo	float	Net horizontal slip low estimate [meters]
nhs_meas_type	nhs_mtype	string	Net horizontal slip measurement type
nhs_style	nhs_style	string	Net horizontal slip style
vs_central_meters	vs_cen	float	Vertical separation preferred value at measurement site [meters]
vs_high_meters	vs_hi	float	Vertical separation high estimate [meters]
vs_low_meters	vs_lo	float	Vertical separation low estimate [meters]
vs_meas_type	vs_mtype	string	Vertical separation measurement type
vs_style	vs_style	string	Vertical separation style: Reverse or Normal
vs_downside	vs_dside	string	Compass description of relative down-dropped side at measurement site
sh_central_meters	sh_cen	float	Scarp height preferred value at measurement site [meters]
sh_high_meters	sh_hi	float	Scarp height high estimate [meters]
sh_low_meters	sh_lo	float	Scarp height low estimate [meters]
sh_meas_type	sh_mtype	string	Scarp height measurement type
sh_style	sh_style	string	Scarp height style: Revere or Normal
sh_downside	sh_dside	float	Compass description of relative down-dropped side at measurement site
ads_central_meters	ads_cen	float	Along-dip slip preferred value at measurement site [meters]
ads_high_meters	ads_hi	float	Along-dip slip high estimate [meters]
ads_low_meters	ads_lo	float	Along-dip slip low estimate [meters]
ads_meas_type	ads_mtype	string	Along-dip slip measurement type
ads_style	ads_style	string	Along-dip slip style: Reverse or Normal
ads_downside	ads_dside	string	Compass description of relative down-dropped side at measurement site
tds_central_meters	tds_cen	float	Three-dimensional preferred value at measurement site [meters]

Full Name (SQL, Flatfiles)	Short Name (SHP, KMZ)	Datatype	Definition
tds_high_meters	tds_hi	float	Three-dimensional high estimate [meters]
tds_low_meters	tds_lo	float	Three-dimensional low estimate [meters]
tds_meas_type	tds_mtype	string	Three-dimensional measurement type
GEO_DS_ID	GEO_DS_ID	integer	Dataset unique identifier for geology data
geology	geology	string	Simple geologic description of measurement site: Young Alluvium (Holocene), Old Alluvium, Undifferentiated Alluvium, or Bedrock
lithology	lithology	string	Full geologic description of measurement site
unit_age	unit_age	string	Epoch or period of geologic unit
distance_to_bedrock_meters	dist2rock	float	Distance to closest mapped bedrock outcrop [meters]
existing_scarp	pre_scarp	integer	Flag = 1 if measurement is on pre-existing scarp; 0 if no pre-existing scarp; -999 if unknown
structure	structure	string	Description of geologic structure, from dataset originator
elevation_meters	elev_m	float	Elevation based on SRTM 1 arc-second (30 meter) resolution digital elevation model; exception: Denali area based on IFSAR digital terrain model resampled to 30-meter resolution [meters]
slope_percent_gaussian_gradient	slope_pct1	float	Ground slope (inclination from horizontal) calculated using SciPy Gaussian gradient model [percent]
slope_percent_gdal_horns_formula	slope_pct2	float	Ground slope (inclination from horizontal) calculated using GDAL Horn's Formula model [percent]
terrain_class	ter_class	integer	Terrain classification code per Iwahashi et al. (2018). 1: steep mountain, rough; 2: steep mountain, smooth; 3: moderate mountain, rough; 4: moderate mountain, smooth; 5: hills, rough in small and large scales; 6: hills, smooth in small scale, rough in large scale; 7: upper large slope; 8: middle large slope; 9: dissected terrace, moderate plateau; 10: slope in and around terrace or plateau; 11: terrace, smooth plateau; 12: alluvial fan, pediment, bajada, pediplain; 13: alluvial plain, pediplain; 14: alluvial or coastal plain, pediplain; 15: alluvial or coastal plain (gentlest), lake plain, playa.
terrain_roughness	ter_rough	integer	Metric for surface irregularity, calculated using GDAL as largest difference between pixel at site and all adjacent pixels

Full Name (SQL, Flatfiles)	Short Name (SHP, KMZ)	Datatype	Definition
topo_position_index	tpi	float	Topographic Position Index (TPI); metric for surface irregularity, calculated using GDAL as the difference between pixel at site and mean of all adjacent pixels; value of zero corresponds to flat topography
terrain_ruggedness_index	tri	float	Terrain Ruggedness Index (TRI); metric for surface irregularity, calculated using GDAL, per Riley et al. (1999), as the sum elevation change between pixel at site and all adjacent pixels; value of zero corresponds to flat terrain
prominence_125_meter_radius	prom125_m	float	Metric for surface irregularity, calculated as the difference between pixel at site and mean of all pixels within 125-meter radius; negative value corresponds to topographic depression, positive value corresponds to topographic high
prominence_250_meter_radius	prom250_m	float	Metric for surface irregularity, calculated as the difference between pixel at site and mean of all pixels within 250-meter radius; negative value corresponds to topographic depression, positive value corresponds to topographic high
prominence_500_meter_radius	prom500_m	float	Metric for surface irregularity, calculated as the difference between pixel at site and mean of all pixels within 500-meter radius; negative value corresponds to topographic depression, positive value corresponds to topographic high
prominence_1000_meter_radius	prom1000_m	float	Metric for surface irregularity, calculated as the difference between pixel at site and mean of all pixels within 1000-meter radius; negative value corresponds to topographic depression, positive value corresponds to topographic high
RUP_DS_ID	RUP_DS_ID	integer	Dataset unique identifier for rupture data for closest mapped rupture line
RUP_ID	RUP_ID	integer	Semi-unique identifier for closest mapped rupture line (for each dataset and each earthquake, values are unique); if measurement rank is Total, Cumulative, or Principal, the closest mapped Principal-rank rupture line is returned
distance_to_rupture_meters	dist2rup	float	Distance to closest mapped rupture line [meters]
rupture_rank	rup_rank	string	Interpretation; rank of closest mapped rupture line, as defined below in "RUPTURES_FLATFILE" definitions

Full Name (SQL, Flatfiles)	Short Name (SHP, KMZ)	Datatype	Definition
fault_dip_central	dip_cen	float	Local fault dip at measurement site [degrees], preferred value
fault_dip_high	dip_hi	float	Local fault dip at measurement site [degrees], high value
fault_dip_low	dip_lo	float	Local fault dip at measurement site [degrees], low value
fault_dip_meas_type	dip_mt	string	Local fault dip at measurement site, measurement type
fault_strike_central	strike_cen	float	Local fault strike at measurement site [degrees], preferred value
fault_strike_high	strike_hi	float	Local fault strike at measurement site [degrees], high value
fault_strike_low	strike_lo	float	Local fault strike at measurement site [degrees], low value
fault_strike_meas_type	strike_mt	string	Local fault strike at measurement site, measurement type
slip_plunge_central	s_plng_cen	float	Local slip plunge at measurement site [degrees], preferred value
slip_plunge_high	s_plng_hi	float	Local slip plunge at measurement site [degrees], high value
slip_plunge_low	s_plng_lo	float	Local slip plunge at measurement site [degrees], low value
slip_plunge_meas_type	s_plng_mt	string	Local slip plunge at measurement site, measurement type
slip_rake_central	s_rake_cen	float	Local slip rake at measurement site [degrees], preferred value
slip_rake_high	s_rake_hi	float	Local slip rake at measurement site [degrees], high value
slip_rake_low	s_rake_lo	float	Local slip rake at measurement site [degrees], low value
slip_rake_meas_type	s_rake_mt	string	Local slip rake at measurement site, measurement type
slip_azimuth_central	s_azm_cen	float	Local slip azimuth at measurement site [degrees], preferred value
slip_azimuth_high	s_azm_hi	float	Local slip azimuth at measurement site [degrees], high value
slip_azimuth_low	s_azm_lo	float	Local slip azimuth at measurement site [degrees], low value
slip_azimuth_meas_type	s_azm_mt	string	Local slip azimuth at measurement site, measurement type
fault_dip_azimuth_central	dip_az_cen	float	Local fault dip azimuth at measurement site [degree +/- compass direction], central value
fault_dip_azimuth_high	dip_az_hi	float	Local fault dip azimuth at measurement site [degree +/- compass direction], high value
fault_dip_azimuth_low	dip_az_lo	float	Local fault dip azimuth at measurement site [degree +/- compass direction], low value
fault_dip_azimuth_meas_type	dip_az_mt	string	Local fault dip azimuth at measurement site, measurement type
u	u	float	Event-specific reference line coordinate system, distance along strike of reference line [meters]
t	t	float	Event-specific reference line coordinate system, perpendicular distance to reference line [meters]

Full Name (SQL, Flatfiles)	Short Name (SHP, KMZ)	Datatype	Definition
measurement_category	meas_cat	string	Generalized measurement type, Point, Profile, or Point Cloud Differencing, as defined below. Point: measurement is based on matching piercing points across a narrow aperture width (generally on the order of < 3 meters) and may not account for off-fault deformation, such as warping; typ. field-based, but can be desktop (air photo, lidar, etc.) Profile: measurement is based on a tens-of-meters-scale profile, comprised of: summed discrete slip on two or more faults; or discrete slip on one or more faults plus continuous deformation; typ. field-based or desktop (air photo, lidar, etc.) Advanced Remote Sensing: measurement is based on large aperture profiles (hundreds-of-meters-scale) generated by InSAR inversion or point cloud differencing of pre- and post-event datasets (such as optical-based remote sensing methods, also referred to as pixel mapping, differential lidar, etc.)
rank	rank	string	Interpretation; measurement categorized as Total, Cumulative, Principal, or Distributed, as defined below. Total: measurement is "profile-based" long profile (hundreds-of-meters-scale), is associated with multiple faults and/or continuous deformation, and is assumed to capture all deformation. Cumulative: measurement is "profile-based" (tens-of-meters-scale) and is associated with multiple faults and/or continuous deformation across the main fault (i.e., sum of principal + distributed). Principal: measurement is associated with main fault breaking ground surface; main fault interpreted based on longer continuity of rupture trace, larger displacements, and usually long-term geologic evidence of faulting; main fault can be expressed as a simple curvilinear trace, segmented left/right stepping en echelon pattern, anastomosing or braided zone, monoclinal warping, etc. Distributed: measurement is associated with a mapped rupture that is not the main fault.
rank_confidence	rank_conf	integer	Database compilers' confidence in assigned rank (1 = high, 2 = low)
hwfw_flag	hwfw_flag	string	Relative location of measurement to principal rupture; applies only to Distributed *rank* measurements and Not Applicable for strike-slip style earthquakes (HW = hanging wall; FW = footwall)

Full Name (SQL, Flatfiles)	Short Name (SHP, KMZ)	Datatype	Definition
recommended_net_preferred_for_analysis_meters	recom_net	float	Interpretation; recommended net (three-dimensional) slip value for using in model development, preferred value, calculated as resultant vector; No Data = -999 [meters]
recommended_net_low_for_analysis_meters	rec_net_lo	float	Interpretation; recommended net (three-dimensional) slip value for using in model development, low value, calculated as resultant vector; No Data = -999 [meters]
recommended_net_high_for_analysis_meters	rec_net_hi	float	Interpretation; recommended net (three-dimensional) slip value for using in model development, high value, calculated as resultant vector; No Data = -999 [meters]
recommended_net_vector_basis	net_basis	string	Vector measurements used to calculate *recommended_net_preferred_for_analysis_meters*
recommended_net_usage_flag	net_flag	string	Interpretation; suggested usage of recommended net values for model development: Keep, Check, or Toss. See *quality_code* field and Table A.2 for more info
quality_code	qual_code	string	Interpretation; list of integer value codes that reflect database compilers' judgment of measurement quality or completeness. See *quality_code* field and Table A.2 for more info
location_id	loc_id	integer	Interpretation; semi-unique identifier for each general measurement location, to be used to identify alternative measurements at a location (for each earthquake, values are unique; field acts as a "bridge" between inferred co-located PT_ID and PT_DS_ID for each earthquake)
group_id	group_id	string	Interpretation; unique identifier for grouping data that are internally compatible (generally based on measurement technique) for each earthquake; see Table A.3 for more info

Table A.2. Measurements Flatfile "Quality Code" explanation.

Quality Code	Explanation	Recommendation[1]	Model Development Usage Flag[1]
1	No known errors or issues (can be any rank or group_id)	Reliable data	Keep
2000	Multiple measurements (same rank and same group_id) available at same location_id (confident[2])	Review available alternative data	Check
2001	Multiple measurements (same rank and same group_id) available at same location_id (inferred[2])	Review available alternative data	Check
3000	Incomplete measurement, lateral slip component might be missing	Use with caution	Check
3001	Incomplete measurement, vertical slip component might be missing	Use with caution	Check
3002	Measurement might be minimum	Use with caution	Check
3003	Measurement might be maximum	Use with caution	Check
3004	Dataset originator quality is low	Use with caution	Check
3005	Deformation might not be tectonic	Use with caution	Check
3006	Incomplete measurement, extensional slip component might be missing	Use with caution	Check
4000	Location might be erroneous	Use with caution	Check
4001	Measurement might be erroneous	Use with caution	Check
5000	Measurement technique might mis-estimate vertical slip component	Use with caution	Check
9000	Other measurement at location_id is more complete	Unreliable data	Toss
9001	No measurement data	Unreliable data	Toss
9002	Incomplete measurement, significant lateral slip unaccounted for	Unreliable data	Toss
9003	Incomplete measurement, significant vertical slip unaccounted for	Unreliable data	Toss
9004	Measurement likely erroneous	Unreliable data	Toss
9005	Location likely erroneous	Unreliable data	Toss
9006	Deformation likely not tectonic	Unreliable data	Toss

[1] Applies to "recommended_net_preferred_for_analysis_meters" column in Measurements Flatfile; included in database for model developers.

[2] Measurements identified as co-located based on documentation from dataset originators (confident) or our evaluation of the reported slip components and site locations (inferred).

Table A.3. Measurements Flatfile "Group ID" explanation.

EQ_ID	eq_name	group_id	measurement_category	rank[1]	Comments
1	Landers	1_01	Point	C, P, D	field-based measurements
1	Landers	1_02	Advanced Remote Sensing	T	optical image correlation
2	HectorMine	2_01	Point	P, D	field-based measurements
2	HectorMine	2_02	Advanced Remote Sensing	T	optical image correlation
2	HectorMine	2_03	Point, Profile	C, D	post-event lidar measurements (acquired ~10 yrs after earthquake)
3	EMC	3_01	Point, Profile	C, P, D	field-based measurements
4	Balochistan	4_01	Point, Profile	C, P, D	post-event high-resolution satellite imagery measurements
4	Balochistan	4_02	Advanced Remote Sensing	T	optical image correlation, densely spaced (~0.5 km average spacing)
4	Balochistan	4_03	Advanced Remote Sensing	T	optical image correlation, broadly spaced (~5.5 km average spacing)
5	Izmit_Kocaeli	5_01	Point, Profile	C, P, D	field-based measurements
6	Borrego	6_01	Point	P, D	field-based measurements
7	Imperial1979	7_01	Point	P, D	field-based measurements
8	SuperstitionHills	8_01	Point	P, D	field-based measurements
9	Kobe	9_01	Point	P, D	field-based measurements
10	Denali	10_01	Point, Profile	C, P, D	field-based measurements
11	Duzce	11_01	Point, Profile	C, P, D	field-based measurements
12	Wenchuan	12_01	Point	P, D	field-based measurements, based on vertical offset
12	Wenchuan	12_02	Point, Profile	C, P, D	field-based measurements, based on scarp height
13	Napa	13_01	Point	P, D	field-based measurements
14	Yushu	14_01	Point	P, D	field-based measurements
15	Hualien	15_01	Point	P, D	field-based measurements
15	Hualien	15_02	Advanced Remote Sensing	T	optical image correlation
16	ChiChi	16_01	Point	P, D	field-based measurements
17	Kumamoto	17_01	Point	P, D	field-based measurements
18	Nagano	18_01	Point, Profile	C, P, D	field-based measurements
19	Kashmir	19_01	Point, Profile	P, D	field-based measurements
20	Kaikoura	20_01	Point, Profile	C, P, D	field-based measurements

EQ_ID	eq_name	group_id	measurement_category	rank[1]	Comments
20	Kaikoura	20_02	Advanced Remote Sensing	T	optical image correlation
21	Darfield	21_01	Point, Profile	C, P	field-based measurements; post-event lidar measurements; post-event high-resolution satellite imagery measurements
22	Parkfield2004	22_01	Point	P, D	field-based measurements
23	Norcia3	23_01	Point	P, D	field-based measurements
24	Hebgen	24_01	Profile	P, D	post-event lidar measurements (acquired ~50 yrs after earthquake), based on vertical offset
24	Hebgen	24_02	Point	P, D	field-based measurements, based on scarp height
25	SanFernando	25_01	Point	P, D	field-based measurements
26	Bohol	26_01	Profile	P, D	field-based measurements
27	Acambay	27_01	Point	P	field-based measurements (acquired ~125 yrs after earthquake)
28	Imperial1940	28_01	Profile	C	field-based measurements
29	Parkfield1966	29_01	Point, Profile	P, D	field-based measurements
30	FairviewPeak	30_01	Profile	P, D	field-based measurements
31	DixieValley	31_01	Profile	P, D	field-based measurements
32	GalwayLake	32_01	Point	P, D	field-based measurements
33	Sonora	33_01	Point, Profile	P, D	field-based measurements (acquired ~125 yrs after earthquake)
34	PleasantValley	34_01	Point, Profile	C, P, D	field-based measurements
35	Kern	35_01	Point	C, P, D	field-based measurements
36	ChalfantValley	36_01	Point	P, D	field-based measurements
37	Zirkuh	37_01	Point	P, D	field-based measurements
38	Petermann	38_01	Point, Profile	C, P, D	field-based measurements
38	Petermann	38_02	Advanced Remote Sensing	T	optical image correlation
39	OwensValley	39_01	Point	P, D	field-based measurements (acquired ~100 yrs after earthquake)
39	OwensValley	39_02	Profile	P, D	post-event lidar measurements (acquired ~125 yrs after earthquake, with some field verification)
40	LagunaSalada	40_01	Point	P, D	field-based measurements (acquired ~125 yrs after earthquake)
41	Iwaki2011	41_01	Point	C, P, D	field-based measurements

EQ_ID	eq_name	group_id	measurement_category	rank[1]	Comments
42	Ridgecrest1	42_01	Point	P, D	field-based measurements
43	Ridgecrest2	43_01	Point	P, D	field-based measurements
44	ElAsnam	44_01	Point	P, D	field-based measurements
45	Cadoux	45_01	Point	P, D	field-based measurements
46	Calingiri	46_01	Point	P, D	field-based measurements
47	MarryatCreek	47_01	Point	P	field-based measurements
48	Meckering	48_01	Point	C, P, D	field-based measurements
49	Pukatja	49_01	Point	P	field-based measurements
50	TennantCreek1	50_01	Point	P	field-based measurements
51	TennantCreek2	51_01	Point	P, D	field-based measurements
52	TennantCreek3	52_01	Point	P	field-based measurements
53	SanMiguel	53_01	Point	P	field-based measurements
54	Yutian	54_01	Point	P, D	field-based measurements
55	Luzon	55_01	Point	P, D	field-based measurements
56	BorahPeak	56_01	Point	C, P, D	field-based measurements
56	BorahPeak	56_02	Profile	C, P, D	post-event lidar measurements (acquired ~40 yrs after earthquake)
57	ElmoreRanch	57_01	Point	P, D	field-based measurements
58	Pisayambo	58_01	Point	P	field-based measurements
58	Pisayambo	58_02	Advanced Remote Sensing	T	InSAR slip inversion
59	Rikuu	59_01	Point	P, D	field-based measurements
60	Mikawa	60_01	Point	P, D	field-based measurements
61	IzuPeninsula	61_01	Point	P, D	field-based measurements
62	IzuOshima	62_01	Point	P, D	field-based measurements
63	IwateInland	63_01	Point	P, D	field-based measurements
64	Edgecumbe	64_01	Point	P, D	field-based measurements
65	Neftegorsk	65_01	Point	C, P, D	field-based measurements
66	ChonKemin	66_01	Point	C, P, D	field-based measurements (acquired ~100 yrs after earthquake)
67	Kunlun_Kokoxili	67_01	Point	C, P	field-based measurements
67	Kunlun_Kokoxili	67_02	Point	P	post-event high-resolution satellite imagery measurements
68	LeTeil	68_01	Point	P, D	field-based measurements

EQ_ID	eq_name	group_id	measurement_category	rank[1]	Comments
68	LeTeil	68_02	Advanced Remote Sensing	D, T	InSAR slip inversion
69	Norcia1	69_01	Point	P, D	field-based measurements
70	HomesteadValley	70_01	Point	P, D	field-based measurements
71	Palu	71_01	Point	P, D	field-based measurements
72	LAquila	72_01	Point	P, D	field-based measurements
73	Spitak	73_01	Point	P	field-based measurements
74	Killari	74_01	Point	P, D	field-based measurements
75	YeniceGonen	75_01	Point	P	field-based measurements

[1] Rank abbreviations as follows: T = Total; C = Cumulative; P = Principal; D = Distributed; See Table 4.2 in main report for more information on the ranking.

2.3 RUPTURES FLATFILE

The Ruptures Flatfile (*.csv format; File #03 in "*FDHI Database flatfiles and related digital products*) contains 32 columns to capture the metadata, raw data, and interpreted data. The main report describes the data collection and data analysis/interpretation procedures. Table A.4 shows the column names in the *.csv flatfile with the column definitions. The equivalent column names in the ESRI shapefile (discussed more in Chapter 3 of this Appendix) are also listed in Table A.4. The information in Table A.4 also contained in the Definitions file (File #01; see Chapter 2.1 of this Appendix).

The Ruptures Flatfile contains ordered coordinate pairs (latitude/longitude or u/t) for each vertex that composes a rupture line. Individual rupture lines for each EQ_ID are identified with the RUP_ID column, and the NODE_ID column contains the vertex order (Figure A.1).

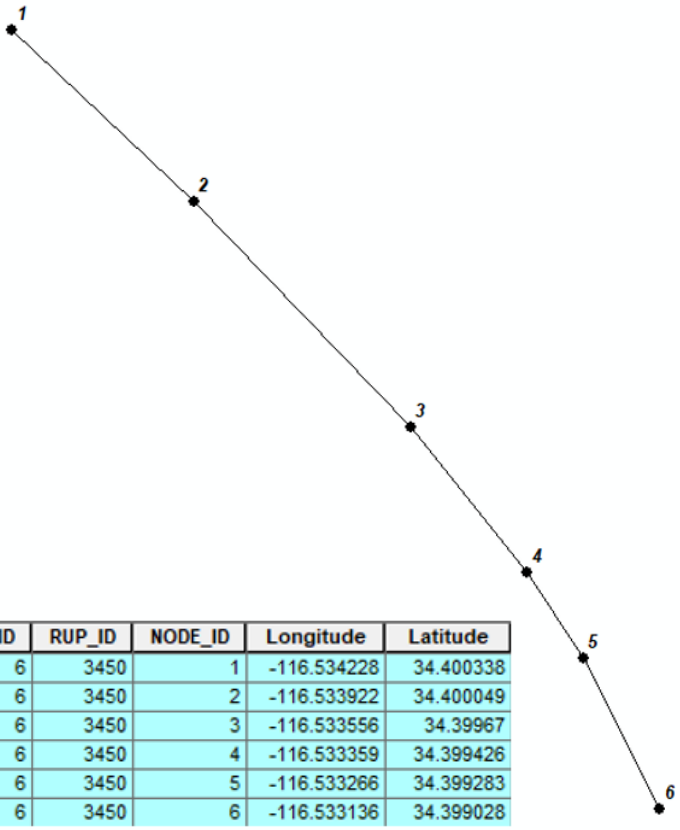

EQ_ID	RUP_DS_ID	RUP_ID	NODE_ID	Longitude	Latitude
1	6	3450	1	-116.534228	34.400338
1	6	3450	2	-116.533922	34.400049
1	6	3450	3	-116.533556	34.39967
1	6	3450	4	-116.533359	34.399426
1	6	3450	5	-116.533266	34.399283
1	6	3450	6	-116.533136	34.399028

Figure A.1. Example reconstruction of rupture linework from Rupture Flatfile.

It is noted that a few earthquakes in the database have alternative rupture line work datasets. These should be treated as alternatives and not supplements. The alternatives are generally related to mapping scale and are discussed in more detail in the main report in Chapter 4.6.1.

Table A.4. Ruptures Flatfile column explanation.

Full Name (SQL, Flatfiles)	Short Name (SHP, KMZ)	Datatype	Definition
index	N/A	integer	Unique row identifier in flatfile for indexing purposes only; not related database primary keys or content
EQ_ID	EQ_ID	integer	Unique identifier for each earthquake
eq_name	eq_name	string	Common name for each earthquake
eq_date	eq_date	string	Earthquake date YYYY-MM-DD
region	region	string	Geographical area of earthquake
magnitude	magnitude	float	Earthquake magnitude
magnitude_type	mag_type	string	Earthquake magnitude type: Mw = moment magnitude; Mwc = moment magnitude derived from centroid moment tensor inversion of long-period surface waves; Mww = moment magnitude derived from centroid moment tensor inversion of W-phase; mB = body-wave magnitude; ML = local magnitude; Ms = surface-wave magnitude; U = unspecified
style	style	string	Dominant earthquake style
multi_event_flag	multievent	integer	Indicates if dataset-event pair captures one or more earthquakes for which data cannot be attributed to individual events (0 = no; 1 = yes, multi-event)
aftershock_flag	aftershock	integer	Indicates if rupture line is known to have ruptured in an aftershock (0 = no; 1 = yes, aftershock)
hypocenter_longitude_degrees	hypo_long	float	Earthquake hypocenter longitude [decimal degrees]
hypocenter_latitude_degrees	hypo_lat	float	Earthquake hypocenter latitude [decimal degrees]
hypocenter_depth_km	hypo_depth	float	Earthquake hypocenter depth [km]
epsg_meters	epsg	integer	Datum and projection identification number per European Petroleum Search Group (EPSG) standard
RUP_DS_ID	RUP_DS_ID	integer	Dataset unique identifier for rupture data
dataset_completion	completion	string	Description of dataset-event pair completion
mapping_scale	map_scale	string	Description of dataset mapping scale
RUP_ID	RUP_ID	integer	Semi-unique identifier for each rupture line (for each dataset and each earthquake, values are unique)

Full Name (SQL, Flatfiles)	Short Name (SHP, KMZ)	Datatype	Definition
NODE_ID	N/A	integer	Semi-unique identifier for each rupture vertex/node (for each dataset and each earthquake and each rupture line, values are unique)
longitude_degrees	longitude	float	Rupture line vertex longitude [decimal degrees]
latitude_degrees	latitude	float	Rupture line vertex latitude [decimal degrees]
line_length_meters	rup_length	float	Length of segment [meters]
end_check	end_check	string	Description of mapping completion for each rupture line
confidence	confidence	string	Location confidence of each rupture line as reported by dataset originator
GEO_DS_ID	GEO_DS_ID	integer	Dataset unique identifier for geology data
geology	geology	string	Simple geologic description of rupture line node/vertex: Young Alluvium (Holocene), Old Alluvium, Undifferentiated Alluvium, or Bedrock
lithology	lithology	string	Full geologic description of rupture node
unit_age	unit_age	string	Epoch or period of geologic unit
u	N/A	float	Event-specific reference line coordinate system, distance along strike of reference line [meters]
t	N/A	float	Event-specific reference line coordinate system, perpendicular distance to reference line [meters]
rank	rank	string	Interpretation; rupture line categorized as Principal or Distributed, as defined below. Principal: line is associated with main fault breaking ground surface, based on longer continuity of rupture trace, larger displacements, and usually long-term geologic evidence of faulting; can be expressed as a simple curvilinear trace, segmented left/right stepping en echelon pattern, anastomosing or braided zone, monoclinal warping, etc. Distributed: line is associated with a mapped rupture that is not the main fault. NoData: rupture dataset cannot be ranked at this time.
rank_confidence	rank_conf	integer	Database compilers' confidence in assigned rank (1 = high, 2 = low)

2.4 EVENT-SPECIFIC COORDINATE SYSTEM (ECS) FLATFILE

The ECS Flatfile (*.csv format; File #04 in *FDHI Database flatfiles and related digital products*) contains 16 columns to capture the metadata, raw data, and analysis results. Chapter 4.5 in the main report describes the development of the ECS. Table A.5 shows the column names in the *.csv flatfile with the column definitions. The equivalent column names in the ESRI shapefile (discussed more in Chapter 3 of this Appendix) are also listed in Table A.5. The information in Table A.5 also contained in the Definitions file (File #01; see Chapter 2.1 of this Appendix).

Similar to the Ruptures Flatfile (Chapter 2.3 of this Appendix), the ECS Flatfile contains ordered coordinate pairs (latitude/longitude or u/t) for each vertex that compose the ECS reference line. There is only one reference line for each earthquake. The NODE_ID column contains the vertex order.

Table A.5. ECS Flatfile column explanation.

Full Name (SQL, Flatfiles)	Short Name (SHP, KMZ)	Datatype	Definition
index	N/A	integer	Unique row identifier in flatfile for indexing purposes only; not related database primary keys or content
EQ_ID	EQ_ID	integer	Unique identifier for each earthquake
eq_name	eq_name	string	Common name for each earthquake
eq_date	eq_date	string	Earthquake date YYYY-MM-DD
region	region	string	Geographical area of earthquake
magnitude	magnitude	float	Earthquake magnitude
magnitude_type	mag_type	string	Earthquake magnitude type: Mw = moment magnitude; Mwc = moment magnitude derived from centroid moment tensor inversion of long-period surface waves; Mww = moment magnitude derived from centroid moment tensor inversion of W-phase; mB = body-wave magnitude; ML = local magnitude; Ms = surface-wave magnitude; U = unspecified
style	style	string	Dominant earthquake style
hypocenter_longitude_degrees	hypo_long	float	Earthquake hypocenter longitude [decimal degrees]
hypocenter_latitude_degrees	hypo_lat	float	Earthquake hypocenter latitude [decimal degrees]
hypocenter_depth_km	hypo_depth	float	Earthquake hypocenter depth [km]
NODE_ID	NODE_ID	integer	Semi-unique identifier for each each ECS linepath (for each earthquake, values are unique)
longitude_degrees	N/A	float	ECS line vertex in geographic coordinates, longitude [decimal degrees]
latitude_degrees	N/A	float	ECS line vertex in geographic coordinates, latitude [decimal degrees]
u	N/A	float	ECS line vertex in ECS coordinates, distance along strike of reference line [meters]
t	N/A	float	ECS line vertex in ECS coordinates, perpendicular distance to reference line [meters]

3 Related Digital Products

The flatfiles (Chapter 2 of this Appendix) are the chief end-user product of the FDHI Database. They are in *.csv format and therefore easily handled by most software and programming languages. For further end-user convenience, the information in the flatfiles is also provided as ESRI shapefiles and compressed Google Earth Keyhole Markup Language files (*.kmz) for use in various Geographic Information System (GIS) software. Finally, we also created data plots of the most used information in the FDHI Database.

3.1 ESRI SHAPEFILES

The ESRI vector file format is commonly referred to as a "shapefile" or *.shp format. It is a proprietary file format owned by ESRI, but the technical specification is documented in a white paper[1]. Importantly, the shapefile format is a multi-file format requiring a minimum of three files (*.shp, *.shx, and *.dbf) to open in any GIS software. For this project, each shapefile set contains eight related files; therefore, the individual shapefile sets are compressed into *.zip files to ensure the related multi-files remain together in the same subdirectory.

The ESRI shapefiles were created directly from the three flatfiles. Accordingly, three ESRI shapefile sets are provided in the *FDHI Database flatfiles and related digital products*: Measurements (File #05), Ruptures (File #06), and ECS (File #07). Because ESRI shapefiles have a ten-character limit on column names, some column names are abbreviated relative to the flatfiles. The shapefile column names are documented in the Definitions file (File #01) and in Tables A.1, A.4, and A.5 of this Appendix.

3.2 GOOGLE EARTH KMZ FILES

The *.kml format was developed for viewing geospatial data in a predecessor to Google Earth. The format uses Keyhole Markup Language, and the files can be compressed (or "zipped") into *.kmz files. To better support end-user needs, we created a *.kmz file for each earthquake in the FDHI Database; therefore, there are 75 *.kmz files in File #08 in *FDHI Database flatfiles and*

[1] ESRI (1998). ESRI Shapefile Technical Description, An ESRI White Paper—July 1998.

related digital products. Note that this is different from the ESRI shapefiles (Chapter 3.1 of this Appendix), which are simply each flatfile converted to a shapefile format.

Figure A.2 shows examples of the nested folder structure in the *.kmz files. The ECS reference linepath, surface ruptures, and measurements are separated or "nested" in the root *.kmz file (Figure A.2A). The nested structure allows users to turn on/off data to suit their viewing needs. Surface ruptures for each earthquake are further divided into Principal and Distributed ranks in the nested folder structure; see Chapter 4.3 in the main report for ranking methodology, and Table A.4 herein for definitions of Principal and Distributed surface ruptures. For events that have multiple surface rupture datasets, the alternative rupture datasets are differentiated by the "RUP_DS_ID" (Figure A.2B) (also see Chapter 2.3 of this Appendix regarding multiple surface rupture datasets). Finally, for events that have incompatible measurements that are separated by the grouping identifier ("group_id"; see Chapter 2.2 of this Appendix), the *.kmz files include nested folders for each "group_id" (Figure A.2C).

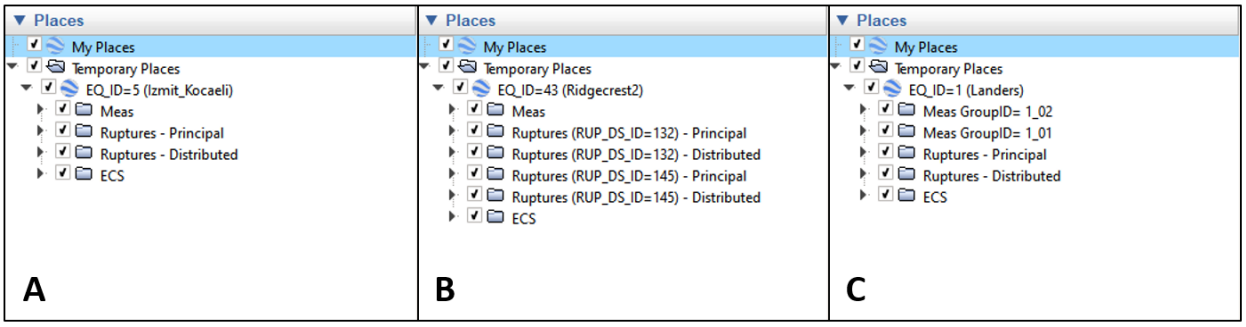

Figure A.2. Example nested file structure for *.kmz files. (A) Example from 1999 **M** 7.51 Izmit-Kocaeli, Turkey earthquake (EQ_ID = 5), representing events with only one measurement group and one surface rupture dataset. (B) Example from 2019 **M** 7.1 Ridgecrest2, California earthquake (EQ_ID = 43), representing events with only one measurement group and alternative surface rupture datasets. (C) Example from 1992 **M** 7.28 Landers, California earthquake (EQ_ID = 1), representing events with only one surface rupture dataset and multiple measurement groupings. See text for discussion on alternative rupture datasets and measurement groupings.

4 Data Plots

To further support quick visualization of the data contained in the FDHI Database, we created data plots directly from the flatfiles. The data plots are presented as HTML Notebooks in an Electronic Supplement to Appendix A. The data plots contain maps of the rupture linework, measurement locations, and ECS reference linepath. The data plots also contain profiles (projected into the ECS u-t coordinate system) of the recommended net slip values, color-coded by amplitude, rank, and geology.

5 Software

The following software versions were used to generate the flatfiles, ESRI shapefiles, Google Earth *.kmz files, and HTML data plots:

- SQLite database engine version 3.14.2 (Hipp, 2020[2])
- Python versions 2.7.15 and 3.7.10
- Python “sqlite3” module version 2.6.0
- Python “pandas” library version 0.18.1
- ESRI ArcMap and ArcGIS Desktop software version 10.7, Advanced license
- Geospatial Data Abstraction Library (GDAL) version 3.3.1
- R version 3.6.3
- R “rmarkdown” module version 2.7

[2] Hipp, R. D. (2020). SQLite. Retrieved from https://www.sqlite.org/index.html.

6 Database Citations

Dataset sources are tracked in the FDHI Database and flatfiles through a dataset identifier column ("DS_ID"). The datasets used in the database are listed below in DS_ID order (not alphabetically), in the following format: "[DS_ID] Citation". The DS_ID identifier is an arbitrary, nonsequential integer. The information below is also contained in the Definitions file (File #01 in *FDHI Database flatfiles and related digital products*; see Chapter 2.1 of this Appendix).

[2] Field, E.H., Biasi, G.P., Bird, P., Dawson, T.E., Felzer, K.R., Jackson, D.D., Johnson, K.M., Jordan, T.H., Madden, C., Michael, A.J., Milner, K.R., Page, M.T., Parsons, T., Powers, P.M., Shaw, B.E., Thatcher, W.R., Weldon, R.J., II, and Zeng, Y., 2013, Uniform California earthquake rupture forecast, version 3 (UCERF3)—The time-independent model: U.S. Geological Survey Open-File Report 2013–1165, 97 p., California Geological Survey Special Report 228, and Southern California Earthquake Center Publication 1792, http://pubs.usgs.gov/of/2013/1165/.

[3] Milliner, C. W. D., Dolan, J. F., Hollingsworth, J., Leprince, S., & Ayoub, F. (2016). Comparison of coseismic near-field and off-fault surface deformation patterns of the 1992 Mw 7.3 Landers and 1999 Mw 7.1 Hector Mine earthquakes: Implications for controls on the distribution of surface strain. Geophysical Research Letters, 43(19).

[6] pers. comm., Dawson, T. to Sarmiento, A. in support of: Petersen, M. D., Dawson, T. E., Chen, R., Cao, T., Wills, C. J., Schwartz, D. P., & Frankel, A. D. (2011). Fault displacement hazard for strike-slip faults. Bulletin of the Seismological Society of America, 101(2), 805-825.

[14] Jennings, C.W., with modifications by Gutierrez, C., Bryant, W., Saucedo, G., and Wills, C., 2010, Geologic map of California: California Geological Survey, Geologic Data Map No. 2, scale 1:750,000.

[16] Padilla y Sánchez, R.J., Domínguez Trejo, I., López Azcárraga, A.G., Mota Nieto, J., Fuentes Menes, A.O., Rosique Naranjo, F., Germán Castelán, E.A., Campos Arriola, S.E., 2013, National Autonomous University of Mexico Tectonic Map of Mexico GIS Project, American Association of Petroleum Geologists GIS Open Files series.

[17] Teran, O. J., Fletcher, J. M., Oskin, M. E., Rockwell, T. K., Hudnut, K. W., Spelz, R. M., ... & Morelan, A. E. (2015). Geologic and structural controls on rupture zone fabric: A field-

based study of the 2010 Mw 7.2 El Mayor–Cucapah earthquake surface rupture. Geosphere, 11(3), 899-920.

[18] Fletcher, J. M., Teran, O. J., Rockwell, T. K., Oskin, M. E., Hudnut, K. W., Mueller, K. J., ... & Fielding, E. J. (2014). Assembly of a large earthquake from a complex fault system: Surface rupture kinematics of the 4 April 2010 El Mayor–Cucapah (Mexico) Mw 7.2 earthquake. Geosphere, 10(4), 797-827.

[19] U.S. Geological Survey (2017). Quaternary fault and fold database for the United States, accessed 2017, from USGS web site: https://earthquake.usgs.gov/hazards/qfaults/.

[20] pers. comm., Kuo, Y.-T. & Yu, W. to Dawson, T., dated 2018-08-29

[22] GNS Science (2018). "2016 Kaikoura Rupture" GIS download, accessed 9 October 2018 [https://data.gns.cri.nz/af/].

[23] Gold, R. D., Reitman, N. G., Briggs, R. W., Barnhart, W. D., Hayes, G. P., & Wilson, E. (2015). On-and off-fault deformation associated with the September 2013 Mw 7.7 Balochistan earthquake: Implications for geologic slip rate measurements. Tectonophysics, 660, 65-78.

[24] Haeussler, P.J. (2009). Surface rupture map of the 2002 M7.9 Denali fault earthquake, Alaska; digital data: U.S. Geological Survey Data Series 422 [http://pubs.usgs.gov/ds/422/].

[25] Wilson, F.H., Hults, C.P., Mull, C.G, and Karl, S.M, comps., 2015, Geologic map of Alaska: U.S. Geological Survey Scientific Investigations Map 3340, pamphlet 196 p., 2 sheets, scale 1:1,584,000, http://dx.doi.org/10.3133/sim3340.

[28] Phillips, W.M. (2011). County Geology and Hazard Maps of Idaho. Digital Databases DD-4, version 6.2011.1, available at [https://www.idahogeology.org/product/dd-4].

[31] Rymer, M. J., Treiman, J. A., Kendrick, K. J., Lienkaemper, J. J., Weldon, R. J., Bilham, R., ... & Irvine, P. J. (2011). Triggered surface slips in southern California associated with the 2010 El Mayor-Cucapah, Baja California, Mexico, earthquake (No. 2010-1333). US Geological Survey.

[32] Kearse, J., Little, T. A., Van Dissen, R. J., Barnes, P. M., Langridge, R., Mountjoy, J., ... & Lamarche, G. (2018). Onshore to offshore ground-surface and seabed rupture of the Jordan–Kekerengu–Needles fault network during the 2016 M w 7.8 Kaikōura earthquake, New Zealand. Bulletin of the Seismological Society of America, 108(3B), 1573-1595.

[33] Langridge, R. M., Rowland, J., Villamor, P., Mountjoy, J., Townsend, D. B., Nissen, E., ... & Hatem, A. E. (2018). Coseismic Rupture and Preliminary Slip Estimates for the Papatea Fault and Its Role in the 2016 Mw 7.8 Kaikōura, New Zealand, Earthquake Coseismic Rupture and Preliminary Slip Estimates for the Papatea Fault. Bulletin of the Seismological Society of America, 108(3B), 1596-1622.

[34] Williams, J. N., Barrell, D. J., Stirling, M. W., Sauer, K. M., Duke, G. C., & Hao, K. X. (2018). Surface rupture of the Hundalee fault during the 2016 M w 7.8 Kaikōura earthquake. Bulletin of the Seismological Society of America, 108(3B), 1540-1555.

[36] pers. comm., Dawson, T. to Sarmiento, A., dated 2018-07-18

[37] Pucci, S., Palyvos, N., Zabci, C., Pantosti, D., & Barchi, M. (2006). Coseismic ruptures and tectonic landforms along the Düzce segment of the North Anatolian Fault Zone (Ms 7.1, November 1999). Journal of Geophysical Research: Solid Earth, 111(B6).

[38] pers. comm., Hartleb, R. to Sarmiento, A., dated 2018-11-27 in support of: Hartleb, R. D., Dolan, J. F., Akyuz, H. S., Dawson, T. E., Tucker, A. Z., Yerli, B., ... & Altunel, E. (2002). Surface rupture and slip distribution along the Karadere segment of the 17 August 1999 Izmit and the western section of the 12 November 1999 Duzce, Turkey, earthquakes. Bulletin of the Seismological Society of America, 92(1), 67-78.

[39] Haeussler, P. J., Schwartz, D. P., Dawson, T. E., Stenner, H. D., Lienkaemper, J. J., Sherrod, B., ... & Personius, S. F. (2004). Surface rupture and slip distribution of the Denali and Totschunda faults in the 3 November 2002 M 7.9 earthquake, Alaska. Bulletin of the Seismological Society of America, 94(6B), S23-S52.

[40] Crone, A. J., Personius, S. F., Craw, P. A., Haeussler, P. J., & Staft, L. A. (2004). The Susitna Glacier thrust fault: Characteristics of surface ruptures on the fault that initiated the 2002 Denali fault earthquake. Bulletin of the Seismological Society of America, 94(6B), S5-S22.

[41] Geological Survey of Japan, AIST (ed.). 2015. Seamless digital geological map of Japan 1: 200,000. May 29, 2015 version. Geological Survey of Japan, National Institute of Advanced Industrial Science and Technology.

[43] pers. comm., Akyuz, S. to Sarmiento, A., dated 2018-12-28 in support of: Akyuz, H. S., Hartleb, R., Barka, A., Altunel, E., Sunal, G., Meyer, B., & Armijo, V. R. (2002). Surface rupture and slip distribution of the 12 November 1999 Duzce earthquake (M 7.1), North Anatolian fault, Bolu, Turkey. Bulletin of the Seismological Society of America, 92(1), 61-66.

[44] Liu-Zeng, J., Zhang, Z., Wen, L., Tapponnier, P., Sun, J., Xing, X., ... & Ji, C. (2009). Co-seismic ruptures of the 12 May 2008, Ms 8.0 Wenchuan earthquake, Sichuan: East-west crustal shortening on oblique, parallel thrusts along the eastern edge of Tibet. Earth and Planetary Science Letters, 286(3-4), 355-370.

[45] Liu-Zeng, J., Wen, L., Sun, J., Zhang, Z., Hu, G., Xing, X., ... & Xu, Q. (2010). Surficial slip and rupture geometry on the Beichuan fault near Hongkou during the Mw 7.9 Wenchuan earthquake, China. Bulletin of the Seismological Society of America, 100(5B), 2615-2650.

[46] Liu-Zeng, J., Sun, J., Wang, P., Hudnut, K. W., Ji, C., Zhang, Z., ... & Wen, L. (2012). Surface ruptures on the transverse Xiaoyudong fault: a significant segment boundary breached during the 2008 Wenchuan earthquake, China. Tectonophysics, 580, 218-241.

[47] pers. comm., Liu-Zeng, J. to Shen, A., dated Winter 2018/Spring 2019

[50] Xu, X., Wen, X., Yu, G., Chen, G., Klinger, Y., Hubbard, J., & Shaw, J. (2009). Coseismic reverse-and oblique-slip surface faulting generated by the 2008 Mw 7.9 Wenchuan earthquake, China. Geology, 37(6), 515-518.

[51] Tan, X. B., Yuan, R. M., Xu, X. W., Chen, G. H., Klinger, Y., Chang, C. P., ... & Li, K. (2012). Complex surface rupturing and related formation mechanisms in the Xiaoyudong area for the 2008 Mw 7.9 Wenchuan Earthquake, China. Journal of Asian Earth Sciences, 58, 132-142.

[52] Xu, X., Chen, W., Ma, W., Yu, G., & Chen, G. (2002). Surface rupture of the Kunlunshan earthquake (Ms 8.1), northern Tibetan plateau, China. Seismological Research Letters, 73(6), 884-892.

[54] pers. comm., Liu-Zeng, J. to Sarmiento, A., dated 2019-03-18

[56] Ponti, D. J., Rosa, C. M., & Blair, J. L. (2019). The Mw 6.0 South Napa earthquake of August 24, 2014--Observations of surface faulting and ground deformation, with recommendations for improving post-earthquake field investigations (No. 2019-1018). US Geological Survey. ... & ... Ponti, D. J., Rosa, C. M., and Blair, J. L.. (2019). Digital datasets documenting fault rupture and ground deformation features produced by the Mw 6.0 South Napa Earthquake of August 24, 2014: U.S. Geological Survey data release, https://doi.org/10.5066/F7P26W84.

[57] Li, C. Y., Pang, J. Z., & Zhang, Z. Q. (2012). Characteristics, geometry, and segmentation of the surface rupture associated with the 14 April 2010 Yushu earthquake, eastern Tibet, china. Bulletin of the Seismological Society of America, 102(4), 1618-1638.

[58] Guo, J., Zheng, J., Guan, B., Fu, B., Shi, P., Du, J., ... & Liu, L. (2012). Coseismic surface rupture structures associated with 2010 Ms 7.1 Yushu earthquake, China. Seismological Research Letters, 83(1), 109-118.

[60] Chen, L., Wang, H., Ran, Y., Sun, X., Su, G., Wang, J., ... & Zhang, X. (2010). The M S 7.1 Yushu earthquake surface rupture and large historical earthquakes on the Garzê-Yushu Fault. Chinese Science Bulletin, 55(31), 3504-3509.

[61] Kuo, Y. T., Wang, Y., Hollingsworth, J., Huang, S. Y., Chuang, R. Y., Lu, C. H., ... & Chang, C. P. (2018). Shallow fault rupture of the Milun fault in the 2018 M w 6.4 Hualien earthquake: A high-resolution approach from optical correlation of Pléiades satellite imagery. Seismological Research Letters, 90(1), 97-107.

[62] Huang, S.-Y., Yen, J.-Y., Wu, B.-L., Yen, I.-C., & Chuang, R. Y. (2019). Investigating the Milun Fault: The coseismic surface rupture zone of the 2018/02/06 ML 6.2 Hualien earthquake, Taiwan. Terrestrial, Atmospheric and Oceanic Sciences, 30, 1-25, doi: 10.3319/ TAO.2018.12.09.03

[63] Huang, S.-Y., Yen, J.-Y., Wu, B.-L., Yen, I.-C., & Chuang, R. Y. (2019). Investigating the Milun Fault: The coseismic surface rupture zone of the 2018/02/06 ML 6.2 Hualien earthquake, Taiwan. Terrestrial, Atmospheric and Oceanic Sciences, 30, 1-25, doi: 10.3319/ TAO.2018.12.09.03

[64] pers. comm., Chun-Hsia Kuo to Andi Shen, dated 2019-05-17, 1:500,000 geological map of Taiwan from Central Geological Survey

[65] Huang, Q.-Y. (1999). Report on the comprehensive disaster investigation of 921 Chi-Chi Earthquake, NCREE.

[66] Lee, Y. H., Hsieh, M. L., Lu, S. D., Shih, T. S., Wu, W. Y., Sugiyama, Y., ... & Kariya, Y. (2003). Slip vectors of the surface rupture of the 1999 Chi-Chi earthquake, western Taiwan. Journal of Structural Geology, 25(11), 1917-1931.

[67] Shirahama, Y., Yoshimi, M., Awata, Y., Maruyama, T., Azuma, T., Miyashita, Y., ... & Otsubo, M. (2016). Characteristics of the surface ruptures associated with the 2016 Kumamoto earthquake sequence, central Kyushu, Japan. Earth, Planets and Space, 68(1), 191. Supplemented with pers. comm., authors to S. Baize.

[68] Okada, S., Ishimura, D., Niwa, Y., & Toda, S. (2015). The First Surface-Rupturing Earthquake in 20 Years on a HERP Active Fault is Not Characteristic: The 2014 M w 6.2 Nagano Event along the Northern Itoigawa–Shizuoka Tectonic Line. Seismological Research Letters, 86(5), 1287-1300.

[69] Katsube, A., Kondo, H., Taniguchi, K., & Kase, Y. (2017). Surface rupture and slip associated with the 2014 Nagano-ken Hokubu earthquake (Mw 6.2). J. Geol. Soc. Japan, 1, 1-21. Supplemented with pers. comm., authors to S. Baize.

[70] pers. comm., Ishimura, D. to Sarmiento, A., dated 2019-03-28 & 2019-04-26, in support of: Ishimura, D., Toda, S., Mukoyama, S., Homma, S. I., Yamaguchi, K., & Takahashi, N. (2019). 3D Surface Displacement and Surface Ruptures Associated with the 2014 M w 6.2 Nagano Earthquake Using Differential Lidar. Bulletin of the Seismological Society of America.

[71] Kaneda, H., Nakata, T., Tsutsumi, H., Kondo, H., Sugito, N., Awata, Y., ... & Yeats, R. S. (2008). Surface rupture of the 2005 Kashmir, Pakistan, earthquake and its active tectonic implications. Bulletin of the Seismological Society of America, 98(2), 521-557.

[73] Zinke, R., Hollingsworth, J., Dolan, J. F., & Van Dissen, R. (2019). Three-Dimensional Surface Deformation in the 2016 MW 7.8 Kaikōura, New Zealand, Earthquake From

Optical Image Correlation: Implications for Strain Localization and Long-Term Evolution of the Pacific-Australian Plate Boundary. Geochemistry, Geophysics, Geosystems, 20(3), 1609-1628.

[74] Heron, D.W. (custodian) 2018: Geological Map of New Zealand 1:250 000. GNS Science Geological Map 1 (2nd ed.). Lower Hutt, New Zealand. GNS Science.

[75] Zinke, R., Hollingsworth, J., & Dolan, J. F. (2014). Surface slip and off-fault deformation patterns in the 2013 MW 7.7 Balochistan, Pakistan earthquake: Implications for controls on the distribution of near-surface coseismic slip. Geochemistry, Geophysics, Geosystems, 15(12), 5034-5050.

[76] Various Italy State Geology Maps a 1:10,000 scale; Marche [http://www.regione.marche.it/Regione-Utile/Paesaggio-Territorio-Urbanistica/Cartografia/Repertorio/Cartageologicaregionale10000], accessed 8 August 2019; Umbria [http://dati.umbria.it/dataset/carta-geologica-dell-umbria], accessed 8 August 2019.

[77] Litchfield, N. J., Van Dissen, R. J., Hornblow, S., Quigley, M. C., & Archibald, G. C. (2014). Detailed analysis of Greendale fault ground surface rupture displacements and geometries. GNS Science.

[78] Quigley, M., Van Dissen, R., Litchfield, N., Villamor, P., Duffy, B., Barrell, D., ... & Noble, D. (2012). Surface rupture during the 2010 Mw 7.1 Darfield (Canterbury) earthquake: Implications for fault rupture dynamics and seismic-hazard analysis. Geology, 40(1), 55-58.

[79] Elliott, J. R., Nissen, E. K., England, P. C., Jackson, J. A., Lamb, S., Li, Z., ... & Parsons, B. (2012). Slip in the 2010–2011 Canterbury earthquakes, New Zealand. Journal of Geophysical Research: Solid Earth, 117(B3).

[80] Villamor, P., Litchfield, N., Barrell, D., Van Dissen, R., Hornblow, S., Quigley, M., ... & Townsend, D. (2012). Map of the 2010 Greendale Fault surface rupture, Canterbury, New Zealand: application to land use planning. New Zealand Journal of Geology and Geophysics, 55(3), 223-230.

[83] Rymer, M. J., Tinsley III, J. C., Treiman, J. A., Arrowsmith, J. R., Clahan, K. B., Rosinski, A. M., ... & Bawden, G. W. (2006). Surface fault slip associated with the 2004 Parkfield, California, earthquake. Bulletin of the Seismological Society of America, 96(4B), S11-S27.

[84] Johnson, K. L., Nissen, E., & Lajoie, L. (2018). Surface Rupture Morphology and Vertical Slip Distribution of the 1959 M w 7.2 Hebgen Lake (Montana) Earthquake From Airborne Lidar Topography. Journal of Geophysical Research: Solid Earth, 123(9), 8229-8248.

[85] O'Neill, J.M., and Christiansen, R.L., 2002, Geologic map of the Hebgen Lake 30' x 60' quadrangle, Beaverhead, Madison, and Gallatin counties, Montana, Park and Teton counties, Wyoming, and Clark and Fremont Counties, Idaho: Montana Bureau of Mines and Geology Open-File Report 464, 21 p., 1 sheet, scale 1:100,000.

[86] Baize, S., Nurminen, F., Sarmiento, A., Dawson, T., Takao, M., Scotti, O., ... & Civico, R. (2019). A Worldwide and Unified Database of Surface Ruptures (SURE) for Fault Displacement Hazard Analyses. Seismological Research Letters.

[87] pers. comm., SURE database updates (in prep.)

[88] Villani, F., Civico, R., Pucci, S., Pizzimenti, L., Nappi, R., De Martini, P. M., ... & Amoroso, S. (2018). A database of the coseismic effects following the 30 October 2016 Norcia earthquake in Central Italy. Scientific data, 5, 180049.

[89] Brozzetti, F., Boncio, P., Cirillo, D., Ferrarini, F., de Nardis, R., Testa, A., ... & Lavecchia, G. (2019). High-resolution field mapping and analysis of the August–October 2016 coseismic surface faulting (central Italy earthquakes): Slip distribution, parameterization, and comparison with global earthquakes. Tectonics, 38(2), 417-439.

[90] Schwartz, D. P., Haeussler, P. J., Seitz, G. G., & Dawson, T. E. (2012). Why the 2002 Denali fault rupture propagated onto the Totschunda fault: Implications for fault branching and seismic hazards. Journal of Geophysical Research: Solid Earth, 117(B11).

[91] Rimando, J. M., Aurelio, M. A., Dianala, J. D. B., Taguibao, K. J. L., Agustin, K. M. C., Berador, A. E. G., & Vasquez, A. A. (2019). Coseismic ground rupture of the October 15, 2013 Magnitude (MW) 7.2 Bohol Earthquake, Bohol Island, Central Philippines. Tectonics.

[92] Klinger, Y., Xu, X., Tapponnier, P., Van der Woerd, J., Lasserre, C., & King, G. (2005). High-resolution satellite imagery mapping of the surface rupture and slip distribution of the M w~ 7.8, 14 November 2001 Kokoxili earthquake, Kunlun fault, northern Tibet, China. Bulletin of the Seismological Society of America, 95(5), 1970-1987.

[93] Urbina, F., & Camacho, H. (1913). La zona megaséismica Acambay-Tixmadeje, estado de México: conmovida el 19 de noviembre de 1912 (Vol. 32). Imprenta y fototipia de la Secretaría de fomento... available at [http://xcaret.igeofcu.unam.mx/bolgeol32.html].

[94] Langridge, R. M., Weldon, R. J., Moya, J. C., & Suárez, G. (2000). Paleoseismology of the 1912 Acambay earthquake and the Acambay-Tixmadejé fault, Trans-Mexican volcanic belt. Journal of Geophysical Research: Solid Earth, 105(B2), 3019-3037.

[95] California Geological Survey (2019). Alquist-Priolo (AP) Earthquake Fault Zones (EFZ) Geographic Information System (GIS) files; available at [http://gmw.conservation.ca.gov/SHP/EZRIM/GIS/], accessed 12/2019.

[96] Rockwell, T. K., & Klinger, Y. (2013). Surface rupture and slip distribution of the 1940 Imperial Valley earthquake, Imperial fault, southern California: Implications for rupture segmentation and dynamics. Bulletin of the Seismological Society of America, 103(2A), 629-640.

[97] Hill, R. L., & Beeby, D. J. (1977). Surface faulting associated with the 5.2 magnitude Galway Lake earthquake of May 31, 1975: Mojave Desert, San Bernardino County, California. Geological Society of America Bulletin, 88(10), 1378-1384.

[98] Caskey, S. J., Wesnousky, S. G., Zhang, P., & Slemmons, D. B. (1996). Surface faulting of the 1954 Fairview Peak (MS 7.2) and Dixie Valley (MS 6.8) earthquakes, central Nevada. Bulletin of the Seismological Society of America, 86(3), 761-787.

[99] Chen, T., Akciz, S. O., Hudnut, K. W., Zhang, D. Z., & Stock, J. M. (2015). Fault-Slip Distribution of the 1999 M w 7.1 Hector Mine Earthquake, California, Estimated from Postearthquake Airborne LiDAR Data. Bulletin of the Seismological Society of America, 105(2A), 776-790.

[100] Sharp, R. V., Budding, K. E., Boatwright, J., Ader, M. J., Bonilla, M. G., Clark, M. M., ... & O'Neill, B. J. (1989). Surface faulting along the Superstition Hills fault zone and nearby faults associated with the earthquakes of 24 November 1987. Bulletin of the Seismological Society of America, 79(2), 252-281.

[103] Langridge, R.M., Ries, W.F., Litchfield, N.J., Villamor, P., Van Dissen, R.J., Barrell, D.J.A., Rattenbury, M.S., Heron, D.W., Haubrock, S., Townsend, D.B., Lee, J.M., Berryman, K.R., Nicol, A., Cox, S.C., Stirling, M.W. (2016). The New Zealand Active Faults Database. New Zealand Journal of Geology and Geophysics 59: 86-96. doi: 10.1080/00288306.2015.1112818.

[104] FDHI Manual Compilation based on the following three sources: {1} California Geological Survey (2019). Alquist-Priolo (AP) Earthquake Fault Zones (EFZ) Geographic Information System (GIS) files; available at [http://gmw.conservation.ca.gov/SHP/EZRIM/GIS/], accessed 12/2019. {2} Rockwell, T. K., & Klinger, Y. (2013). Surface rupture and slip distribution of the 1940 Imperial Valley earthquake, Imperial fault, southern California: Implications for rupture segmentation and dynamics. Bulletin of the Seismological Society of America, 103(2A), 629-640. {3} Trifunac, M. D., & Brune, J. N. (1970). Complexity of energy release during the Imperial Valley, California, earthquake of 1940. Bulletin of the Seismological Society of America, 60(1), 137-160.

[106] Howell, A., Nissen, E., Stahl, T., Clark, K., Kearse, J., Van Dissen, R., ... & Jones, K. (2020). 3D surface displacements during the 2016 MW 7.8 Kaikōura earthquake (New Zealand) from photogrammetry-derived point clouds. Journal of Geophysical Research: Solid Earth.

[107] FDHI Manual Compilation based on the following two sources: {1} GNS Science (2018). "2016 Kaikoura Rupture" GIS download, accessed 9 October 2018 [https://data.gns.cri.nz/af/]. {2} Zinke, R., Hollingsworth, J., Dolan, J. F., & Van Dissen, R. (2019). Three-Dimensional Surface Deformation in the 2016 MW 7.8 Kaikōura, New Zealand, Earthquake From Optical Image Correlation: Implications for Strain Localization and Long-Term Evolution of the Pacific-Australian Plate Boundary. Geochemistry, Geophysics, Geosystems, 20(3), 1609-1628.

[108] Brown, R. D. Jr. and J. G. Vedder (1966). Surface tectonic fractures along the San Andreas Fault, The Parkfield-Cholame California earthquakes of June-August 1966, U.S. Geological Survey Professional Paper 579.

[110] Suter, M. (2015). Rupture of the Pitáycachi fault in the 1887 Mw 7.5 Sonora, Mexico earthquake (southern Basin-and-Range Province): Rupture kinematics and epicenter inferred from rupture branching patterns. Journal of Geophysical Research: Solid Earth, 120(1), 617-641.

[111] Suter, M. (2008). Structural configuration of the Teras fault (southern Basin and Range Province) and its rupture in the 3 May 1887 Mw 7.5 Sonora, Mexico earthquake. Revista Mexicana de Ciencias Geológicas, 25(1), 179-195.

[112] Suter, M. (2008). Structural configuration of the Otates fault (southern Basin and Range Province) and its rupture in the 3 May 1887 Mw 7.5 Sonora, Mexico, earthquake. Bulletin of the Seismological Society of America, 98(6), 2879-2893.

[113] pers. comm., Suter, M. to Sarmiento, A., dated 2020-05-20, in support of: Suter 2008a, 2008b, 2015

[114] Woodward-Lundgren & Associates, 1974, Summary report—Basis for pipeline design for active-fault crossings for the Trans-Alaska Pipeline System: unpublished report prepared for Alyeska Pipeline Service Company, Houston, Texas, 115 p.

[115] Bartow, J.A. (1984). Geologic map and cross sections of the southeastern margin of the San Joaquin Valley, California: U.S. Geological Miscellaneous Investigations Series Map I-1496, Scale 1:125,000 [https://ngmdb.usgs.gov/Prodesc/proddesc_22.htm].

[116] pers. comm., Thompson, S. to Sarmiento, A., dated 2020-05-26

[117] Wallace, R. E., Bonilla, M. G., & Villalobos, H. A. (1984). Faulting related to the 1915 earthquakes in Pleasant Valley, Nevada: U.S. Geological Survey Professional Paper 1247-A,B [https://pubs.er.usgs.gov/publication/pp1274AB].

[118] Raymond, O. L., & Retter, A. J. (2012). Surface Geology of Australia 1:1 million scale dataset, 2012 edition (digital dataset). Geoscience Australia, Canberra, available at [https://ecat.ga.gov.au/geonetwork/srv/eng/catalog.search#/metadata/74619].

[119] Crone, A. J., Machette, M. N., Bonilla, M. G., Lienkaemper, J. J., Pierce, K. L., Scott, W. E., & Bucknam, R. C. (1987). Surface faulting accompanying the Borah Peak earthquake and segmentation of the Lost River fault, central Idaho. Bulletin of the Seismological Society of America, 77(3), 739-770.

[120] Gold, R. D., Clark, D., Barnhart, W. D., King, T., Quigley, M., & Briggs, R. W. (2019). Surface rupture and distributed deformation revealed by optical satellite imagery: The intraplate 2016 Mw 6.0 Petermann Ranges earthquake, Australia. Geophysical Research Letters, 46(17-18), 10394-10403.

[122] Buwalda, J. P. & St Amand, P. (1955). Geologic Effects of Arvin-Tehachapi Earthquake, California Div. of Mines. Bull, 171, 41-56.

[123] Francesca, F. M. (2020). Surface rupture dataset of 18 normal and strike-slip events (Version 1.0) [Data set]. Zenodo. http://doi.org/10.5281/zenodo.3666192

[124] Berberian, M., Jackson, J. A., Qorashi, M., Khatib, M. M., Priestley, K., Talebian, M., & Ghafuri-Ashtiani, M. (1999). The 1997 May 10 Zirkuh (Qa'enat) earthquake (M w 7.2): faulting along the Sistan suture zone of eastern Iran. Geophysical Journal International, 136(3), 671-694.

[125] Kahle, J. E., Bryant, W. A., & Hart, E. W. (1986). Fault rupture associated with the July 21, 1986 Chalfant Valley earthquake. Mono and Inyo counties, California: California Geology, 39(11), 243-245.

[126] Lienkaemper, J. J., Pezzopane, S. K., Clark, M. M., & Rymer, M. J. (1987). Fault fractures formed in association with the 1986 Chalfant Valley, California, earthquake sequence: preliminary report. Bulletin of the Seismological Society of America, 77(1), 297-305.

[127] FDHI Manual Compilation based on the following two sources: {1} Lienkaemper, J. J., Pezzopane, S. K., Clark, M. M., & Rymer, M. J. (1987). Fault fractures formed in association with the 1986 Chalfant Valley, California, earthquake sequence: preliminary report. Bulletin of the Seismological Society of America, 77(1), 297-305. {2} dePolo, C. M., & Ramelli, A. R. (1987). Preliminary report on surface fractures along the White Mountains fault zone associated with the July 1986 Chalfant Valley earthquake sequence. Bulletin of the Seismological Society of America, 77(1), 290-296.

[128] pers. comm., Haddon, E. to Sarmiento, A., dated 2020-03-05 in support of: Haddon, E. K., Amos, C. B., Zielke, O., Jayko, A. S., & Bürgmann, R. (2016). Surface slip during large Owens Valley earthquakes. Geochemistry, Geophysics, Geosystems, 17(6), 2239-2269.

[129] Beanland, S., & Clark, M. M. (1994). The Owens Valley fault zone, eastern California, and surface faulting associated with the 1872 earthquake: U.S. Geological Survey Bulletin 1982 [https://pubs.er.usgs.gov/publication/b1982].

[130] Rockwell, T. K., Fletcher, J. M., Teran, O. J., Hernandez, A. P., Mueller, K. J., Salisbury, J. B., ... & Štěpančíková, P. (2015). Reassessment of the 1892 Laguna Salada Earthquake: Fault Kinematics and Rupture Patterns. Bulletin of the Seismological Society of America, 105(6), 2885-2893.

[131] Toda, S., & Tsutsumi, H. (2013). Simultaneous reactivation of two, subparallel, inland normal faults during the M w 6.6 11 April 2011 Iwaki earthquake triggered by the M w 9.0 Tohoku-oki, Japan, earthquake. Bulletin of the Seismological Society of America, 103(2B), 1584-1602.

[132] DuRoss, C. B., Gold, R. D., Dawson, T. E., Scharer, K. M., Kendrick, K. J., Akciz, S. O., ... & Blair, L. (2020). Surface Displacement Distributions for the July 2019 Ridgecrest, California, Earthquake Ruptures. Bulletin of the Seismological Society of America.

[133] Philibosian, B., Thompson Jobe, J., Chupik, C., Dawson, T., Bennett, S., Kendrick, K., DuRoss, C., Gold, R., Ladinsky, T., Haddon, E., Pierce, I., Swanson, B., and Seitz, G. (2020). Pre-existing features associated with active faulting in the vicinity of the 2019 Ridgecrest, California earthquake sequence: U.S. Geological Survey data release, https://doi.org/10.5066/P9ENA24Y.

[134] Philip, H., & Meghraoui, M. (1983). Structural analysis and interpretation of the surface deformations of the El Asnam earthquake of October 10, 1980. Tectonics, 2(1), 17-49.

[135] Yielding, G., Jackson, J. A., King, G. C. P., Sinvhal, H., Vita-Finzi, C., & Wood, R. M. (1981). Relations between surface deformation, fault geometry, seismicity, and rupture characteristics during the El Asnam (Algeria) earthquake of 10 October 1980. Earth and Planetary Science Letters, 56, 287-304.

[136] King, T. R., Quigley, M., & Clark, D. (2019). Surface-rupturing historical earthquakes in Australia and their environmental effects: new insights from re-analyses of observational data. Geosciences, 9(10), 408.

[137] Shor Jr, G. G., & Roberts, E. (1958). San Miguel, Baja California Norte, earthquakes of February, 1956: A field report. Bulletin of the Seismological Society of America, 48(2), 101-116.

[139] Harvey, T. W. (1985). Geology of the San Miguel fault zone, northern Baja California, Mexico, Masters Thesis, San Diego State University, San Diego, California, 330 pp.

[140] Mizoguchi, K., Uehara, S. I., & Ueta, K. (2012). Surface Fault Ruptures and Slip Distributions of the M w 6.6 11 April 2011 Hamadoori, Fukushima Prefecture, Northeast Japan, Earthquake. Bulletin of the Seismological Society of America, 102(5), 1949-1956.

[141] FDHI Manual Compilation based on the following two sources: {1} Toda, S., & Tsutsumi, H. (2013). Simultaneous reactivation of two, subparallel, inland normal faults during the M w 6.6 11 April 2011 Iwaki earthquake triggered by the M w 9.0 Tohoku-oki, Japan,

earthquake. Bulletin of the Seismological Society of America, 103(2B), 1584-1602. {2} Mizoguchi, K., Uehara, S. I., & Ueta, K. (2012). Surface Fault Ruptures and Slip Distributions of the M w 6.6 11 April 2011 Hamadoori, Fukushima Prefecture, Northeast Japan, Earthquake. Bulletin of the Seismological Society of America, 102(5), 1949-1956.

[142] FDHI Manual Compilation based on the following two sources: {1} Baize, S., Nurminen, F., Sarmiento, A., Dawson, T., Takao, M., Scotti, O., ... & Civico, R. (2019). A Worldwide and Unified Database of Surface Ruptures (SURE) for Fault Displacement Hazard Analyses. Seismological Research Letters. {2} pers. comm., Kuo, Y.-T. & Yu, W. to Dawson, T., dated 2018-08-29.

[143] USGS (1964). The Hebgen Lake, Montana, earthquake of August 17, 1959, U.S. Geological Survey Professional Paper 435.

[144] Rockwell, T. K., Lindvall, S., Dawson, T., Langridge, R., Lettis, W., & Klinger, Y. (2002). Lateral offsets on surveyed cultural features resulting from the 1999 Izmit and Duzce earthquakes, Turkey. Bulletin of the Seismological Society of America, 92(1), 79-94.

[145] Ponti, D. J., Blair, J. L., Rosa, C. M., Thomas, K., Pickering, A. J., Akciz, S., ... & Barth, N. (2020). Documentation of Surface Fault Rupture and Ground-Deformation Features Produced by the 4 and 5 July 2019 M w 6.4 and M w 7.1 Ridgecrest Earthquake Sequence. Seismological Society of America, 91(5), 2942-2959.

[146] pers. comm., Liu-Zeng, J. to Shen, A., dated July 2020

[147] Li, H., Pan, J., Lin, A., Sun, Z., Liu, D., Zhang, J., ... & Gong, Z. (2016). Coseismic Surface Ruptures Associated with the 2014 Mw 6.9 Yutian Earthquake on the Altyn Tagh Fault, Tibetan Plateau. Bulletin of the Seismological Society of America, 106(2), 595-608.

[148] Nakata, T., Tsutsumi, H., Punongbayan, R. S., Rimando, R. E., Daligdig, J. A., Daag, A. S., & Besana, G. M. (1996). Surface fault ruptures of the 1990 Luzon earthquake, Philippines. Special Publication No, 25.

[149] Vincent, K.R. (1995). Implications for models of fault behavior from earthquake surface displacement along adjacent segments of the Lost Ri ver fault, Idaho: PhD. Dissertation, University of Arizona, 152 p.

[150] FDHI Manual Compilation based on the following two sources: {1} Crone, A. J., Machette, M. N., Bonilla, M. G., Lienkaemper, J. J., Pierce, K. L., Scott, W. E., & Bucknam, R. C. (1987). Surface faulting accompanying the Borah Peak earthquake and segmentation of the Lost River fault, central Idaho. Bulletin of the Seismological Society of America, 77(3), 739-770. {2} Vincent, K.R. (1995). Implications for models of fault behavior from earthquake surface displacement along adjacent segments of the Lost River fault, Idaho: PhD. Dissertation, University of Arizona, 152 p.

[151] DuRoss, C. B., Bunds, M. P., Gold, R. D., Briggs, R. W., Reitman, N. G., Personius, S. F., & Toké, N. A. (2019). Variable normal-fault rupture behavior, northern Lost River fault zone, Idaho, USA. Geosphere, 15(6), 1869-1892.

[152] pers. comm., Arrowsmith, R. to Sarmiento, A., dated 2020-09-18 in support of: Arrowsmith, J. R., Crosby, C. J., Korzhenkov, A. M., Mamyrov, E., Povolotskaya, I., Guralnik, B., & Landgraf, A. (2017). Surface rupture of the 1911 Kebin (Chon–Kemin) earthquake, Northern Tien Shan, Kyrgyzstan. Geological Society, London, Special Publications, 432(1), 233-253.

[153] pers. comm., Boncio, P. to Sarmiento, A., dated 2020-09-16

[154] pers. comm., Pinegina, T. & Kozhurin, A. to Arcos, B., dated 2020-06-14

[155] Goto, H., Tsutsumi, H., Toda, S., & Kumahara, Y. (2017). Geomorphic features of surface ruptures associated with the 2016 Kumamoto earthquake in and around the downtown of Kumamoto City, and implications on triggered slip along active faults. Earth, Planets and Space, 69(1), 26.

[156] FDHI Manual Compilation based on the following two sources: {1} Shirahama, Y., Yoshimi, M., Awata, Y., Maruyama, T., Azuma, T., Miyashita, Y., ... & Otsubo, M. (2016). Characteristics of the surface ruptures associated with the 2016 Kumamoto earthquake sequence, central Kyushu, Japan. Earth, Planets and Space, 68(1), 191. Supplemented with pers. comm., authors to S. Baize. {2} Goto, H., Tsutsumi, H., Toda, S., & Kumahara, Y. (2017). Geomorphic features of surface ruptures associated with the 2016 Kumamoto earthquake in and around the downtown of Kumamoto City, and implications on triggered slip along active faults. Earth, Planets and Space, 69(1), 26.

[157] FDHI Manual Compilation based on the following two sources: {1} Johnson, K. L., Nissen, E., & Lajoie, L. (2018). Surface Rupture Morphology and Vertical Slip Distribution of the 1959 M w 7.2 Hebgen Lake (Montana) Earthquake From Airborne Lidar Topography. Journal of Geophysical Research: Solid Earth, 123(9), 8229-8248. {2} USGS (1964). The Hebgen Lake, Montana, earthquake of August 17, 1959, U.S. Geological Survey Professional Paper 435.

[158] Nurminen, F., Boncio, P., Visini, F., Pace, B., Valentini, A., Baize, S., & Scotti, O. (2020). Probability of occurrence and displacement regression of distributed surface rupturing for reverse earthquakes. Frontiers in Earth Science.

[159] Duman, T. Y., Emre, O., Dogan, A., & Ozalp, S. (2005). Step-over and bend structures along the 1999 Duzce earthquake surface rupture, North Anatolian fault, Turkey. Bulletin of the Seismological Society of America, 95(4), 1250-1262.

[160] FDHI Manual Compilation based on the following three sources: {1} pers. comm., Akyuz, S. to Sarmiento, A., dated 2018-12-28 in support of: Akyuz, H. S., Hartleb, R., Barka, A., Altunel, E., Sunal, G., Meyer, B., & Armijo, V. R. (2002). Surface rupture and slip

distribution of the 12 November 1999 Duzce earthquake (M 7.1), North Anatolian fault, Bolu, Turkey. Bulletin of the Seismological Society of America, 92(1), 61-66.. {2} pers. comm., Dawson, T. to Sarmiento, A., dated 2018-07-18. {3} Duman, T. Y., Emre, O., Dogan, A., & Ozalp, S. (2005). Step-over and bend structures along the 1999 Duzce earthquake surface rupture, North Anatolian fault, Turkey. Bulletin of the Seismological Society of America, 95(4), 1250-1262.

[161] Trifunac, M. D., & Brune, J. N. (1970). Complexity of energy release during the Imperial Valley, California, earthquake of 1940. Bulletin of the Seismological Society of America, 60(1), 137-160.

[162] pers. comm., Dawson, T. to Sarmiento, A., dated 2021-05-05

[165] Fu, B., Awata, Y., Du, J., Ninomiya, Y., & He, W. (2005). Complex geometry and segmentation of the surface rupture associated with the 14 November 2001 great Kunlun earthquake, northern Tibet, China. Tectonophysics, 407(1-2), 43-63.

[167] FDHI Manual Compilation based on the following two sources: {1} California Geological Survey (2019). Alquist-Priolo (AP) Earthquake Fault Zones (EFZ) Geographic Information System (GIS) files; available at [http://gmw.conservation.ca.gov/SHP/EZRIM/GIS/], accessed 12/2019. {2} Bonilla, M. G., J. M. Buchanan, R. O. Castle, M. M. Clark, V. A. Frizell, R. M. Gulliver, F. K. Miller, J. P. Pinkerton, D. C. Ross, R. V. Sharp, R. F. Yerkes, and J. I. Ziony (1971). Surface faulting, U.S. Geological Survey Professional Paper 733, 55-76.

[168] Hill, R. L., Treiman, J. A., Given, J. W., Pechman, J. C., McMillan, J. R., & Ebel, J. E. (1980). Geologic study of the Homestead Valley earthquake swarm of March 15, 1979. California Geology, 33(3), 60-67.

[169] Wu, D., Ren, Z., Liu, J., Chen, J., Guo, P., Yin, G., ... & Yang, X. (2021). Coseismic surface rupture during the 2018 Mw 7.5 Palu earthquake, Sulawesi Island, Indonesia. Bulletin, 133(5-6), 1157-1166.

[170] Jaya, A., Nishikawa, O., & Jumadil, S. (2019). Distribution and morphology of the surface ruptures of the 2018 Donggala–Palu earthquake, Central Sulawesi, Indonesia. Earth, Planets and Space, 71(1), 1-13.

[171] Natawidjaja, D. H., Daryono, M. R., Prasetya, G., Liu, P. L., Hananto, N. D., Kongko, W., ... & Tawil, S. (2021). The 2018 M w7. 5 Palu ‘supershear’earthquake ruptures geological fault's multisegment separated by large bends: results from integrating field measurements, LiDAR, swath bathymetry and seismic-reflection data. Geophysical Journal International, 224(2), 985-1002.

[172] Bureau de Recherches Geologiques et Minieres (BGRM) (2004). Descriptif des cartes geologiques a 1/50 000 format "vecteurs": Rapport BRGM/R P-53473- FR, available at

[http://infoterre.brgm.fr/formulaire/telechargement-cartes-geologiques-departementales-150-000-bd-charm-50].

[173] Nurminen, F., Boncio, P., Visini, F., Pace, B., Valentini, A., Baize, S., & Scotti, O. (2020). Probability of occurrence and displacement regression of distributed surface rupturing for reverse earthquakes. Frontiers in Earth Science, 8, 456.

[174] Rajendran, C. P., Rajendran, K., & John, B. (1996). The 1993 Killari (Latur), central India, earthquake: An example of fault reactivation in the Precambrian crust. Geology, 24(7), 651-654.

[175] Kurcer, A., Ozalp, S., Ozdemi, E., Guldogan, C. U., & Duman, T. Y. (2019). Active tectonic and paleoseismologic characteristics of the Yenice-Gönen fault, NW Turkey, in light of the 18 March 1953 Yenice-Gönen Earthquake (Ms=7.2). Bulletin of the Mineral Research and Exploration, 159(159), 29-62.